Ore Geology Reviews 158 (2023) 105484

Contents lists available at ScienceDirect

Ore Geology Reviews

journal homepage: www.elsevier.com/locate/oregeorev

Evolution of pegmatite recorded by zoned garnet from the No. 9 dike in the Jiajika Li polymetallic deposit, eastern Tibetan plateau

Wen Winston Zhao [a], Mei-Fu Zhou [a,b,*], Zheng Zhao [c], Xin-Fu Zhao [a]

[a] School of Earth Resources, China University of Geosciences, Wuhan 430074, China
[b] State Key Laboratory of Ore Deposit Geochemistry, Institute of Geochemistry, Chinese Academy of Sciences, Guiyang 550081, China
[c] Institute of Mineral Resources, Chinese Academy of Geological Sciences, Beijing 100037, China

ARTICLE INFO

Keywords:
Garnet
Trace elements mapping
U-Pb dating
LA-ICP-MS
Pegmatite
Jiajika

ABSTRACT

Granitic pegmatites can be extremely rich in Li, an important metal for modern industries. Being the Asia's largest hard-rock Li polymetallic deposit, the Jiajika Li deposit is associated with numerous pegmatite dikes in the eastern Tibetan Plateau. The major Li resources in Jiajika are mainly hosted in fine-grained phases of pegmatite dikes. In this study, samples were collected from the typically zoned No. 9 dike, which inwardly consists of fine-grained albite phase, medium-grained albite phase, coarse-grained albite-microline phase, massive microline phase and massive quartz phase. Garnet is one of the common accessory minerals in the fine-grained albite phase. We report the first in-situ LA-ICP-MS U-Pb age of garnet from pegmatite dikes, yielding an age of 216.7 ± 5.9 Ma, which is consistent with the age of the associated granitic pluton. Combined with published isotopic dating results in Jiajika, two age groups can be identified: ~210 to ~ 220 Ma and ~ 190 to ~ 200 Ma, which are suspected to be resulted from two stages of thermal events, probably separate pulses of pegmatitic melts. The late pulse of melts might be responsible for the weak deformation of garnet grains and Fe-enriched rims along the deformed boundaries. The early pulse of melts derived from the Majingzi-Jiajijiami granitic pluton shows an indistinct time path from granite, to fine-grained phases, to medium- to coarse-grained phases, which resulted in the trace elemental core-rim textures within individual garnet grains. The garnet cores have typically higher trace element concentrations than the rims, and the boundaries between cores and rims are usually sharp and sinuous, which are proposed to record the amalgamation, dissolution and reprecipitation processes. The growth of cores was not in equilibrium with other phases by strong undercooling, and thus inherited the initial Li signature of the incipient pegmatitic melts, which can be up to 373 ppm. Accordingly, it implies that Li and other incompatible element contents of the incipient pegmatitic melts in Jiajiaka could be enriched in a significant amount at the early stage, which may, to some extent, explain why major Li resources are hosted in very-fine to fine-grained phases in Jiajika.

1. Introduction

Granitic pegmatites can be extremely rich in lithium (Li), an important metal in nuclear, electronic, optical ceramic, and glass industries (Linnen et al., 2012). It has some common features such as graphic textures and sharply increasing sizes of minerals from fine- to medium-grained massive and layered phases to interior coarse-grained phases (London, 2014). Such zoning patterns are thought to be resulted from the evolution of the incipient pegmatitic melts, which are proposed to be crystal-free, low-viscous, Li- and flux-rich and generally derived from the associated S-type granites (Černý et al., 2005; London, 2014; Simmons and Webber, 2008; Thomas et al., 2012). Finally, it is not until Li is saturated involving the interaction of multiple melt/fluid/solid phases that Li-aluminosilicates precipitate and accumulate to be economic ores (London, 2016; Maneta et al., 2015). However, due to the huge crystal sizes of pegmatite minerals and multi-stage magmatic-hydrothermal processes, the nature and Li contents of the incipient pegmatitic melts are not well known. In addition. the textural evidence of multi-phase crystal-melt interactions leading to Li saturation is lacking and seldomly discussed.

Being one of the typical accessory minerals in granitic pegmatites, the geochemical characteristics and origin of garnet in pegmatite receive wide attention. It is because granitic pegmatites, similar to associated granites, were not formed at great depths under which garnet was

* Corresponding author.

https://doi.org/10.1016/j.oregeorev.2023.105484
Received 8 November 2022; Received in revised form 19 April 2023; Accepted 4 May 2023
Available online 9 May 2023
0169-1368/© 2023 The Author(s). Published by Elsevier B.V. This is an open access article under the CC BY-NC-ND license (http://creativecommons.org/licenses/by-nc-nd/4.0/).

thought to nucleate and grow (Stevens et al., 2007). Numerous studies show that garnets in pegmatite are compositionally commonly Mn-rich and Ca-poor, distinctively different from granitic garnets (e.g., Samadi et al., 2014; Whitworth, 1992; Yu et al., 2021). It is generally proposed that garnet in pegmatite has Mn-rich cores and Fe-rich rims, and Mn contents in these garnets increase towards the interior of pegmatite dikes (Arredondo et al., 2001; Baldwin and von Knorring, 1983; Morgan and London, 1999; Wang et al., 2003b). However, as one of the early studies, Manning (1983) shows that the distribution of major elements in individual garnet is complex and variable, especially those in fine-grained phases where both unzoned and zoned grains may occur. One plausible explanation is that growth zoning in major elements is commonly reset by volume diffusion, which is particularly efficient at high temperatures for major elements with high diffusion coefficients, which may totally or partially obliterate their initial features (e.g., Chakraborty and Ganguly, 1992). Trace elements generally have lower diffusion coefficients compared to major elements, so they can be a more robust geochemical tracer, and also provide insight into some mineral reaction histories that exclude the major elements (e.g., Pyle and Spear, 2003). Several studies show that trace elements in individual garnet grains are mostly enriched in the cores and depleted in the rims (Samadi et al., 2014; Wang et al., 2003a; Yu et al., 2021), which seems to be decoupled from those of major elements. This issue currently received little attention. Therefore, a detailed study of the trace element distribution within individual garnet grains in pegmatite is key to understand the pegmatite-forming processes.

The Jiajika Li deposit in eastern Tibetan Plateau is the largest hard-rock Li deposit in Asia, and contains about 2.9 million tonnes of Li_2O (Fu et al., 2019). The major Li resources are hosted in very-fine- to fine-grained phases in pegmatite dikes in this deposit (Fu et al., 2019; London, 2016). Garnet is also widely present in pegmatite dikes in Jiajika (Fu et al., 2019; Tang and Wu, 1984). Several isotopic ages of mica, zircon, cassiterite and columbite acquired by different approaches constrain the formation of pegmatites to be ~ 189 to ~ 218 Ma, which can be linked to the formation of gneiss domes by emplacement of the associated granite (Dai et al., 2019; Hao et al., 2015; Li et al., 2020; Tang and Wu, 1984; Wang et al., 2005; Xu et al., 2020). Recent Li isotopic studies in the Jiajika deposit also show that mineralized pegmatite dikes

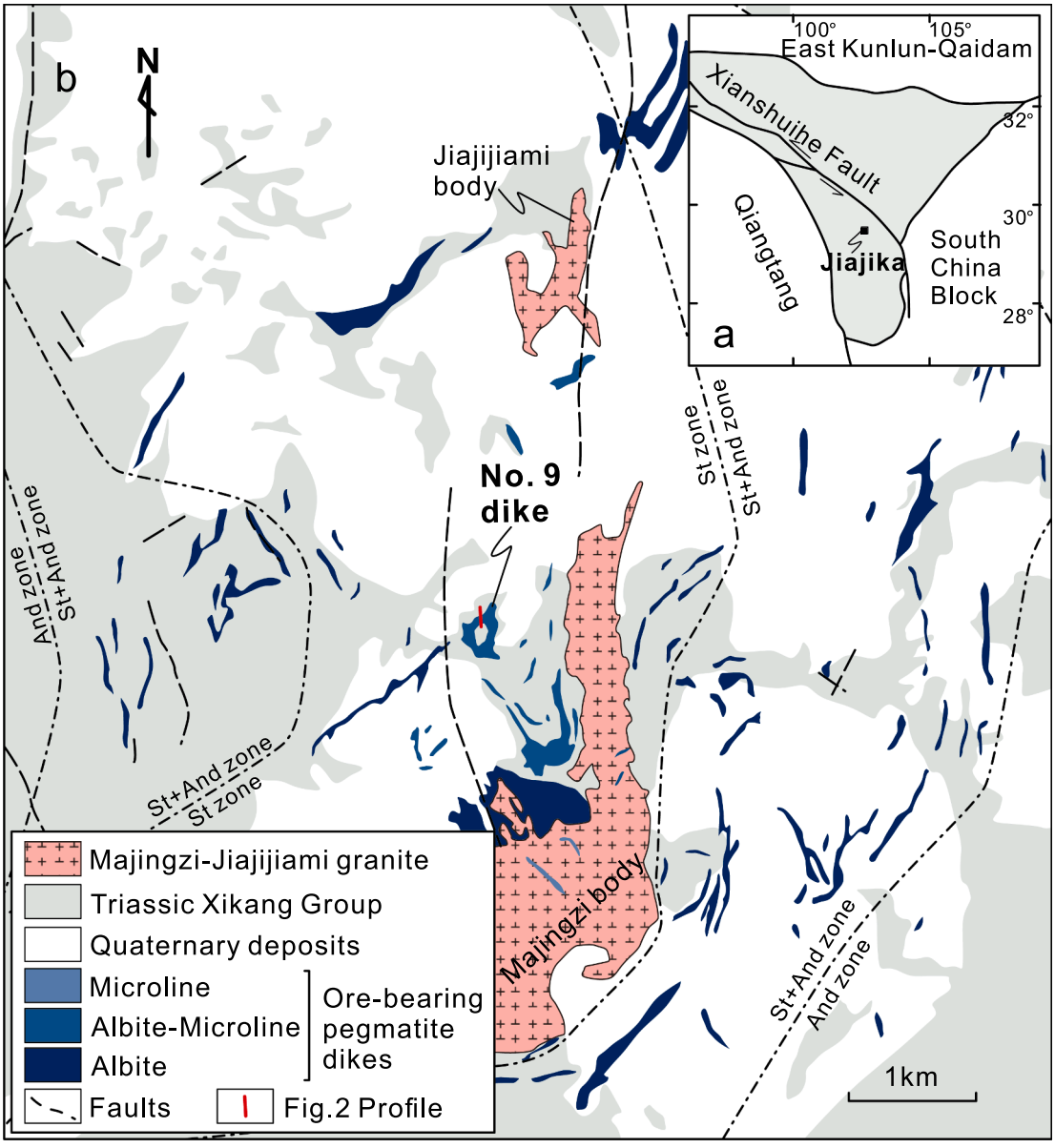

Fig. 1. a: Simplified geological map showing the location of the jiajika deposit in theSongpan-Ganze Orogenic Belt (SGOB) (modified after Xu et al., 2020). b: Simplified geological map of the Jiajika pegmatite Li deposit (modified after Fu et al., 2019; Tang and Wu, 1984).

are closely related to the associated granite that could be derived from a Li-rich sources (Zhang et al., 2021; Zhao et al., 2022). By investigation of melt inclusions in the marginal phase of the associated granite via a hydrothermal diamond anvil cell and Raman spectroscopy, Li and Li (2014) and Li and Chou (2015) show that the incipient pegmatitic melts separated from the granitic melts are extremely hydrous and flux-rich, and Deng et al. (2022) propose that Li contents in the pegmatitic melts could be up to ~ 1000 ppm. Li and Chou (2016) and Li and Chou (2017) also note that daughter minerals in melt inclusions within spodumene were crystallized from entrapped carbonate- and silica-rich aqueous solutions. However, the history from intrusion of incipient pegmatitic melts to precipitation of ore minerals is poorly known.

In this contribution, we report a U-Pb age and major and trace element mapping of garnet from the fine-grained phase of the No. 9 dike in the Jiajika deposit, to show complex chemical zoning patterns within individual garnet grains and interactions of multi-phases resulting in the Li mineralization and pegmatitic textures. The aim of this study is to understand the origin of garnet in pegmatite in the context of several current models and its implication for the formation of pegmatite deposits.

2. The Jiajika Li deposit

Several Li pegmatite deposits were discovered in the Songpan-Ganze Orogenic Belt (SGOB) of the eastern margin of the Tibetan Plateau (Xu et al., 2020), bounded by the East Kunlun-Qaidam terrane to the north, the Qiangtang terrane to the south, and the South China Block to the east (Fig. 1a). The SGOB was formed during the Middle to Late Triassic closure of the paleo-Tethys Ocean (Yin and Harrison, 2000). The basement of the eastern SGOB is composed of a Neoproterozoic crystalline complex (1–0.75 Ga), covered by thick (5–15 km) middle-upper Triassic turbiditic sedimentary succession of the Xikang Group (Roger et al., 2010). The thick Triassic metasedimentary succession was intruded by numerous granitic plutons mainly with ages of 228–195 Ma (Yuan et al., 2010). The eastern SGOB underwent extensive, early Indosinian deformation as indicated by a basal decollement and fold-thrust structures in the overlying sedimentary rocks. Previously, the SGOB was divided into the north Songpan and south Ganze sub-terranes along the NW-trending Xianshuihe fault, which formed at ~ 30 Ma in response to the India-Asia collision (Roger et al., 1995; Xu et al., 1992).

In the Jiajika deposit, the Triassic Majingzi-Jiajijiami granitic pluton intruded the Triassic succession along the plunge of the Jiajika anticline. This pluton is composed of the Majingzi body in the south and the Jiajijiami body in the north (Fig. 1b). The fine-grained phases of the granite, exposed on the surface, contain plagioclase, K-feldspar, quartz, biotite, muscovite and rare spodumene. Geochemically, the granite belongs to high-K calc-alkaline peraluminous S-type granite, possibly derived from partial melting of the crustal pelite during late Triassic (Hao et al., 2015; Li et al., 2020; Liang et al., 2016). The country rocks are mainly schists, which have a protolith of mudstones and sandstones of the Xikang Group. Away from the granitic pluton, it can be generally divided into the staurolite, staurolite + andalusite, andalusite, and biotite metamorphic zones (Fu et al., 2019; Xu et al., 2020). The NW-SE-trending dome-like Jiajika anticline, accompanied by a series of NW-SE-trending faults, constitutes the main tectonic framework in this area.

The Jiajika deposit consists of>500 pegmatite dikes, distributed in an area of about 60 km^2 (Fig. 1b). Based on the abundance of microline and albite, the pegmatite dikes are generally zoned as microline, microline-albite, and albite (including albite-spodumene and albite-lepidolite) types away from the Majingzi-Jiajijiami granitic pluton (Fu et al., 2019; Tang and Wu, 1984). The ore-bearing pegmatite dikes are mostly hosted in the staurolite and staurolite-andalusite metamorphic zones, and controlled by the pre-existing NE-SW- and NW-SE-trending shear zones or contemporaneous conjugate joint and fissure sets. These pegmatite dikes are generally 100 to 500 m long with a maximum length of 1450 m, 1 to 10 m thick with a maximum thickness of 630 m, and 50 to 300 m deep with a maximum depth of>500 m, and typically occur as tabular sills or lenticular bodies, parallel or subparallel to the foliation, indicating an early deformation that formed the obvious foliations and a late deformation in which tabular dikes or irregular masses cut the earlier foliation (Fu et al., 2019). The No. 9 dike occurs in the upper part of the dome-like Jiajika anticline due to emplacement of the Majingzi-Jiajijiami granitic pluton, and is controlled by shear zones along the beddings of the country rocks. Based on mineral assemblages and petrography, it can be divided into the fine-grained albite phase, medium-grained albite phase, coarse-grained albite-microline phase, massive microline phase and massive quartz phase (Fig. 2a). The fine-grained and medium-grained phases have 30 ~ 40% quartz and 40 ~ 60% albite, with subordinate muscovite and microline. The coarse-grained albite-microline phase contains 20 ~ 35% quartz, 20 ~ 40% albite, and 20 ~ 40% microline, with subordinate muscovite. The massive microline and quartz phases are dominated by microline (70 ~ 90%) and quartz (>90%), respectively. The main ore minerals in the No. 9 dike are beryl, columbite-tantalite, cassiterite, lepidolite and spodumene, with accessory minerals of tourmaline and garnet, mostly hosted in the fine-grained albite phase (Tang and Wu, 1984). The schist along the contact to the fine-grained albite phase has a mineral assemblage of the upper greenschist facies with tourmaline, cordierite and sericite-chlorite, and the sharp increase of Li contents to the boundary (Tang and Wu, 1984).

In this study, samples were collected from the fine-grained albite phase in the No. 9 dike (Fig. 2b). The samples primarily consist of albite and quartz, where albite grains are enlongated and subhedral to anhedral in shape, and quartz grains are generally anhedral and clustered (Fig. 3a). It is obvious that albite grains are much finer than quartz grains, and show typical lineation around those quartz clusters. Garnet and tourmaline are mostly in the albite domains (Fig. 3b). The garnet usually occurs as separated grains or occasionally as clusters of two or three grains (Fig. 3c). The garnet grains are tiny ranging from 50 to 500 μm, and subhedral to euhedral in shape (Fig. 3c-e). Rounded quartz and subordinate tourmaline inclusions are commonly hosted in the garnet rims (Fig. 3e,h). Ore minerals, like beryl, cassiterite, lepidolite and columbite, are generally intergrown with garnet, tourmaline and garnet, paralleling to the albite lineation (Fig. 3f-h). Minor microcline occurs in the interstitials among albite grains and are in irregular shapes (Fig. 3h).

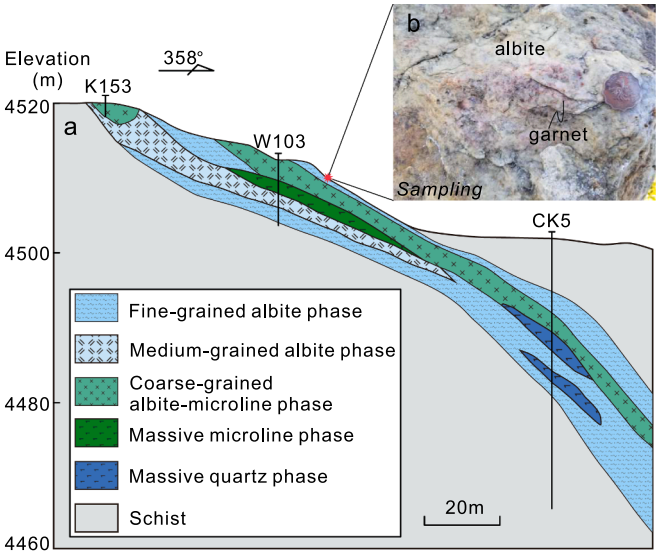

Fig. 2. a: A profile showing different zones of the no. 9 dike (modified after Tang and Wu, 1984). b: A field photo showing the sampling location.

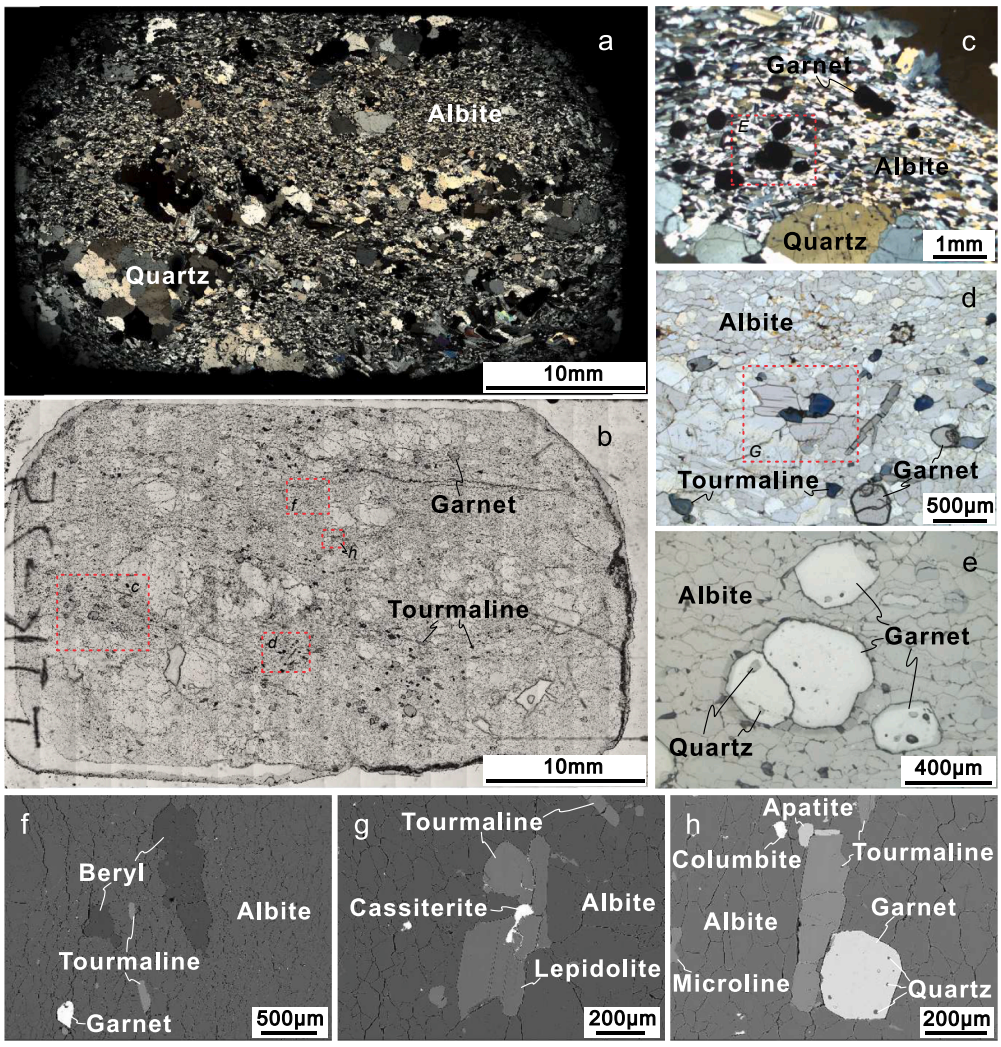

Fig. 3. Microscopic photos of samples. a: under cross-polarized light. b: under plane-polarized light. c: under cross-polarized light. d: under plane-polarized light. e: under reflected light. f-h: back scattered electron images under SEM.

3. Analytical methods

3.1. EMPA elemental analyses

Elemental spot analyses of minerals were performed using a JEOL JXA-8230 electron probe microanalyzer with four wavelength-dispersive spectrometers at the Center for Global Tectonics, School of Earth Sciences, China University of Geosciences, Wuhan. The operating conditions were described in Wang et al. (2019) and Ning et al. (2019) in detail. For spot analyses, 15 kV accelerating voltage, 20nA probe current, and a 1 μm beam diameter had been used. Dwell times were 10 s on element peaks and half that on background locations adjacent to peaks. Raw x-ray intensities were corrected using a ZAF (atomic number, absorption, fluorescence) correction procedure. A series of natural and synthetic SPI standards were utilized and changed based on the analyzing minerals. The following standards were used: pyrope garnet (Fe, Al), diopside (Ca, Mg), rhodonite (Mn), olivine (Si) and rutile (Ti).

3.2. Electron backscattered diffraction analyses

The mechanically polished thin section was examined in a Philips XL30 SEM using a forescatter detector system to collect OC images, and electron backscatter diffraction to measure crystallographic orientations. Misorientation magnitudes of $> 1^{\circ}$ can be quantified using EBSD, although misorientation axes cannot be measured accurately for such small misorientations (Prior, 1999). The presence of smaller misorientations can be verified by comparing EBSD patterns, but the misorientations cannot be quantified because they are smaller than the error in a single lattice orientation measurement.

3.3. LA-ICP-MS U-Pb isotopic dating

Uranium-Pb isotope analyses were performed on garnet using a GeoLasPro 193 nm ArF excimer laser (CompexPro 102F, Coherent) coupled to a Thermo Scientific Element XR sector field ICP-MS at the State Key Laboratory of Ore Deposit Geochemistry, Institute of Geochemistry, Chinese Academy of Sciences, Guiyang. Instrument conditions are the same as reported in Tang et al. (2021). Laser beam diameter, fluencies and repetition rates are 32 μm, 3 J/cm^2 and 5 Hz, respectively. Each analysis consists of 20 s background acquisition followed by approximately 30 s sample ablation. Five to eight pulses of pre-ablation were performed in each analysis. Zircon 91,500 was used as primary standard material, and garnet Willsboro was used as the secondary standard for monitoring the precision and accuracy of the U-Pb dating results. The data collected from ICP-MS of both laboratories were processed off-line using the ICPMSDataCal software, for calibration, background correction, and floating of integration signal (Liu et al., 2010). Spots that were not contaminated by mineral and fluid inclusions were used for further age calculations. The Isoplot program was used to calculate U-Pb ages and finish the Tera-Wasserburg Concordia to obtain

the lower intercept ages (Ludwig, 2001). The obtained weighted average $^{206}Pb/^{238}U$ age of Willsboro garnet is 1024 ± 14 Ma in this study, consistent with the reference age of 1022 ± 16 Ma (Seman et al., 2017).

3.4. LA-ICP-MS spot and mapping analyses

Major and trace element concentrations of garnet were measured by LA-ICP-MS on polished thin sections at the Ore deposit and Exploration Centre, Hefei University of Technology. The analyses were carried out on an Agilent 7900 Quadrupole ICP-MS coupled to a Photon Machines Analyte HE 193-nm ArF Excimer Laser Ablation system equipped. Argon was used as the make-up gas and mixed with the carrier gas via a T-connector before entering the ICP (Ning et al., 2017; Wang et al., 2017). For elemental spot analyses, each analysis was performed by a uniform spot size diameter of 30 mm at 8 Hz with energy of ~ 4 J/cm^2 for 40 s after measuring the gas blank for 20 s. Standard reference materials BCR-2G, NIST 612, and NIST 610, were used as external standards to plot calibration curve. The preferred values of element concentrations for the USGS reference glasses are from the GeoReM database (https://georem.mpch-mainz.gwdg.de/). Standard reference materials were run after each 10–15 unknowns; detection limits were calculated for each element in each spot analysis. The off-line data processing was performed using ICPMSDataCal (Liu et al., 2010). Trace element compositions of garnet were calibrated against multiple-references materials without applying internal standardization. The sum of all element concentrations expressed as oxide (according to their oxidation states present in the silicate) are considered to be 100 % m/m. For elemental mapping, element maps were created by ablating sets of parallel line rasters in a grid across the sample. A beam size of 15–40 μm and scan speeds of 15–40 μm/s (equal to beam size) were used. A laser repetition of 7 Hz was selected at a constant energy output in an energy density of ~ 3 J/cm^2 at the target. A 20-s background acquisition was acquired at the start of scanning, and to allow for cell wash-out, gas stabilization, and computer processing, a delay of 20 s was used after ablation. Reference materials NIST 610 and GSE-1G at the start and end of each mapping was analyzed for data calibration. Images were compiled and processed using the program LIMS (Wang et al., 2017; Xiao et al., 2018). For each raster and every element, the average background was subtracted from its corresponding raster, and the rasters were compiled into a 2-D image displaying combined background/drift corrected intensity for each element (Wang et al., 2017).

4. Analytical results

4.1. Composition and zoning of garnet

Major and trace elements of garnet from the Jiajika deposit are listed in Supplementary Tables 1 and 2. The garnet grains examined are essentially almandine-spessartine solid solutions. Garnet varies widely in composition from $Alm_{29}Spe_{71}$ to $Alm_{60}Spe_{39}$, with minor andradite + grossular (0.6–1.5%) and pyrope (0–0.3%). Garnet grains generally show Mn-rich cores and Fe-rich rims, and the components of andradite, grossular and pyrope show roughly negative correlations with spessartine and positive with almandine. The garnet grains have variable rare earth elements (REEs) concentrations ranging from 2.4 to 120 ppm, and have chondrite-normalized patterns with LREE-depletion and HREE-enrichment, with positive Eu anomalies (Fig. 4a). The garnet cores generally show higher HREE than those of rims, but both show low Er_N/Yb_N and Dy_N/Yb_N (Fig. 4b). By laser spot analyses, trace elements typically have higher concentrations in the cores than those of the rims, and show positive correlation with each other (Fig. 4c). To be specific, Li concentrations in the garnet samples range from 67 ppm to 373 ppm by spot analyses (Supplementary Table 2).

In elemental maps, major and trace elements of garnet grains show decoupled zoning patterns (Fig. 5). Although spot analyses reveal correlations between major and trace elements between different garnet grains, in an individual garnet grain, the trace element zoning patterns are obviously disconnected with those major element patterns. For major elements, Ca, Al and Si are generally homogenous, while Fe, Mn and Mg show different domains with smooth boundaries. Iron and Mg are positively correlated, which are both negatively correlated with Mn that is generally enriched as cores. Trace elements generally show similar patterns with sharp and irregular core-rim boundaries. In the cores, it is patchy and contains domains depleted in trace elements, usually in elongated, rounded shapes. It should be noted that for some aggregated grains, the cores seem to be aggregating and fusing together. The rims that are typically depleted in all trace elements, and showing weak rhythmic patterns as recorded by Y and Sc. It should be noted that those enclosed quartz and tourmaline are mainly in the rims, and irregular tiny pores are generally in the cores (Fig. 5a-c). Two profiles (labeled in Fig. 5a) of Li contents in individual garnet grains are shown in Fig. 6, which were generated directly by the program LIMS based on mapping results (Wang et al., 2017; Xiao et al., 2018). It indicates that

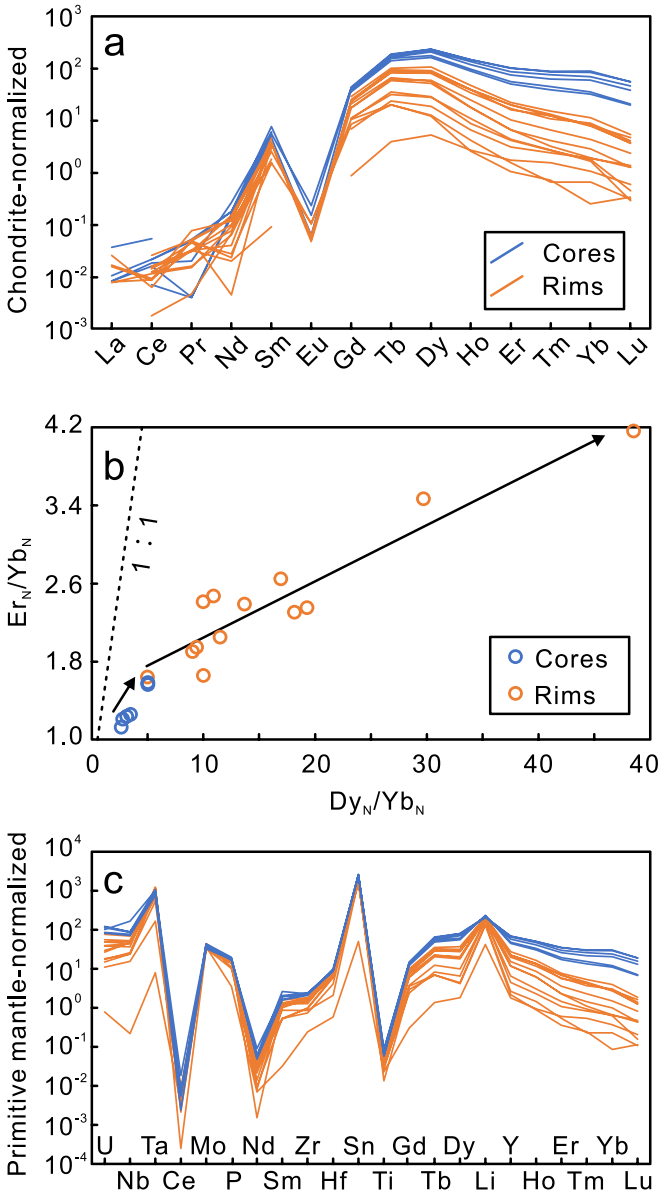

Fig. 4. a: Chondrite-normalized REE patterns. b: Yb_N/Er_N vs Yb_N/Dy_N. c: Primitive mantle normalized spider diagram. Trace elemental compositions of garnet grains acquired by LA-ICP-MS spot analyses. Normalization data from Sun and McDonough (1989).

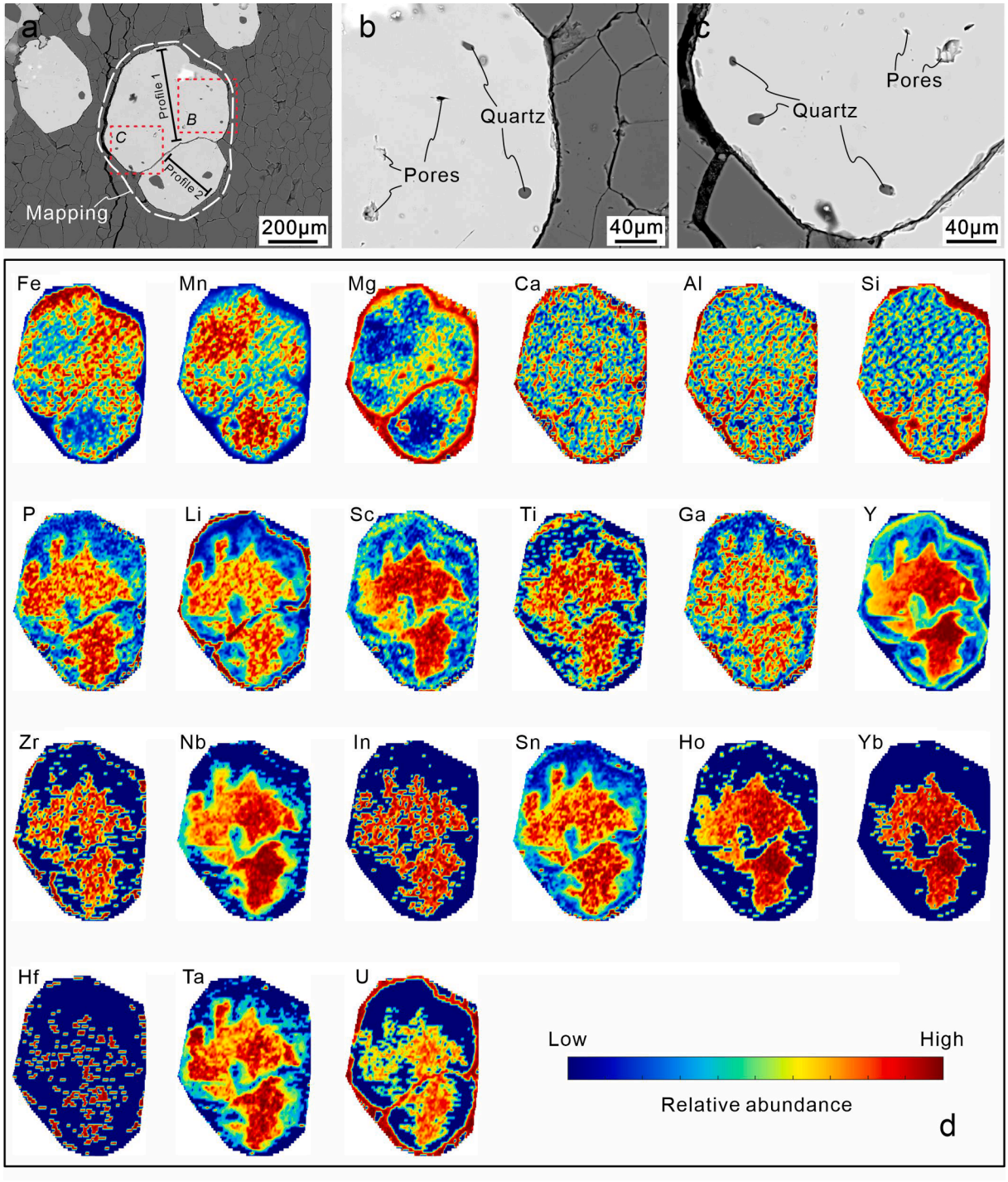

Fig. 5. a-c: Back scattered electron images of targeted garnet grains under SEM. d: major and trace elemental maps acquired by LA-ICP-MS.

the cores generally have ~ 270 to 450 ppm Li and the rims have ~ 50 to ~ 200 ppm Li by mapping analyses, which are both in agreement with the trends revealed by the spot analyses.

4.2. Crystallographic orientation of garnet

The orientation contrast (OC) images of garnet grains that outlined in Fig. 5a were shown in Fig. 7. The individual garnet grains show two to three substructures. The crystallographic orientation within one grain is rotated less than 1°, indicating that the mismatches across cell walls tend to be small. Those low-angle boundaries likely developed during post-(and possibly syn-) crystallization deformation (e.g., Prior et al., 2000), which is distinguishable from those composed of polycrystals that are separated by high-angle boundaries (e.g., Whitney and Seaton, 2010).

4.3. U-Pb dating of garnet

Uranium-lead isotopic data of garnet are listed in Supplementary Table 3. Uranium contents of garnet grains for in-situ dating range from 0.17 to 3.6 ppm. The cores generally show higher U contents than those of the rims. Due to the low U contents in the rims, the uncertainties of ages are generally greater than those cores. Although the core and rim of

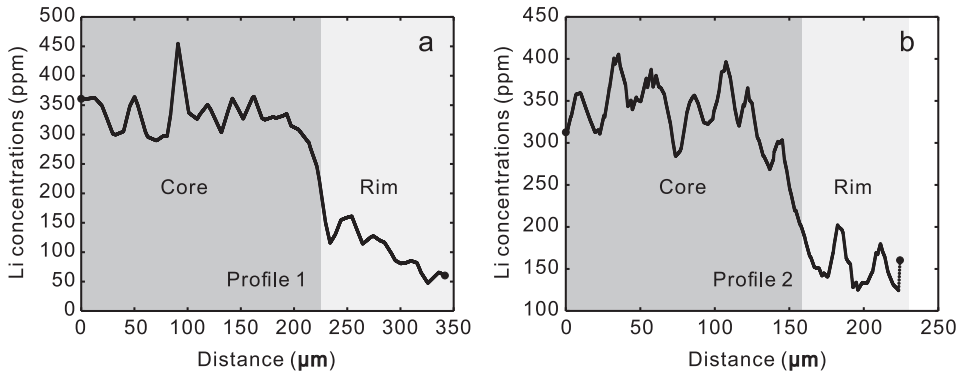

Fig. 6. Lithium content profiles within individual garnet grains generated by the program LIMS from the mapping results. Profiles are labeled in Fig. 5a.

garnet show typically different concentrations of U, they do not have distinguished age within errors, implying the core and rim were formed within a short period. A total of 27 analyses yielded discordant U-Pb ages and produced a lower intercept $^{206}Pb/^{238}U$ age of 216.7 ± 5.9 Ma (MSWD = 1.19) (Fig. 8).

5. Discussion

5.1. Time of pegmatite formation

Dating the formation of pegmatite is challengeable due to its complicated evolution history, but it is also key to understand the origin and mineralization of pegmatite. Several previous studies have constrained the age of the Majingzi-Jiajijiami granitic pluton to be ~ 214 to 223 Ma and pegmatite to be ~ 189 to 217 Ma (Table 1). It should be noted that the Ar-Ar and Rb-Sr ages for pegmatite (~189 to ~ 200 Ma) and granite (~214 Ma) are mostly younger than U-Pb ages of ~ 198 to ~ 217 Ma for pegmatite and ~ 223 Ma for granite (Dai et al., 2019; Hao et al., 2015; Li et al., 2020; Tang and Wu, 1984; Wang et al., 2005). It may be due to the relatively low closure temperature of Ar-Ar and Rb-Sr systems in most minerals than those of U-Pb systems, and thus those ages by Ar-Ar and Rb-Sr methods might be reset by late thermal processes and record time of the late thermal events (Chiaradia et al., 2013). Accordingly, the younger age group, including the young cassiterite U-Pb dating of 198.0 ± 4.4 Ma for the No. 133 dike and zircon U-Pb dating of 186.7 ± 5.3 Ma for the No. X03 dike (Dai et al., 2019; Li et al., 2020), may represent late thermal events in Jiajika as discussed in the next section (Fig. 9).

In terms of U-Pb dating results, Hao et al. (2015) constrained the newly-discovered No. X03 dike to be 216 ± 2 Ma and 214 ± 2 Ma by zircon and columbite-tantalite, respectively, and the granite age to be 223 ± 1 Ma by zircon. Most recently, Dai et al. (2019) constrained the fine-grained and medium- to coarse-grained phases of No. 308 dike to be 217 ± 1.1 Ma by zircon and 211 ± 4.6 Ma by cassiterite, respectively. Li et al. (2020) provided zircon U-Pb ages of 212.9 ± 5.9 Ma and 206.0 ± 3.2 Ma for Majingzi and Jiajijiami granitic bodies, respectively, which further proves the long evolution history of the Majingzi-Jiajijiami granite. In this study, we obtained the U-Pb age of garnet from the fine-grained phase of No. 9 dike to be 217.4 ± 5.7 Ma (Fig. 8). It is worth noting that, although these U-Pb ages are mostly in agreement with each other within errors, it seems that there is a younging trend from fine-grained phases of pegmatite dikes to medium- to coarse-grained phases of pegmatite dikes, which is consistent with the ages of the granite (Table 1; Fig. 9). It confirms the linkage between the Majingzi-Jiajijiami granitic pluton and the mineralized pegmatitic dikes in Jiajika.

5.2. Origin of garnet and formation of elemental zonings

As constrained by ages, garnet formation is linked with the magmatic processes related to the emplacement of the Majingzi-Jiajijiami granitic pluton. Accordingly, the pegmatite garnet may be: 1) direct crystallization products of pegmatitic melts derived from the Majingzi-Jiajijiami pluton; or 2) inherited xenocrysts from the original country-rock contact metamorphic assemblages. However, there are little outlier metamorphic inclusions in the garnet grains, and the temperature of pegmatitic melts are usually too low to completely interact with those metamorphosed country rocks. Additionally, the garnet in magmatic origin generally has high MnO (>12 wt%) and low CaO (<~2%) (e.g., Bonzi et al., 2023; Samadi et al., 2014), and garnet in study has MnO contents of 16.5 ~ 30.0 wt% and CaO contents of 0.20 ~ 0.41 wt%, thus precluding the inherited metamorphic origin.

The typical features of garnet grains in Jiajika are the rounded to euhedral shapes and the incorporation of tiny rounded quartz grains and occasionally tourmaline grains (Fig. 3e,h and 5b,c). These features are similar to garnet grains in granites, which are interpreted to be formed in granitic melts via dissolution-reprecipitation, re-equilibration and amalgamation processes (Taylor and Stevens, 2010). In Jiajika, trace elements in garnet cores might be inherited from melts, by which the cores grew before trace element equilibration was reached (e.g., Spandler et al., 2011; George et al., 2018). Most garnet grains have small pores (Fig. 5b,c) and the embayed shape of core-rim boundaries (Fig. 5d), reflecting that the dissolution-reprecipitation processes may happen (e.g., Putnis, 2009).

Another feature of trace element patterns for the contacted garnet grains is the connected trace-element-rich cores between two grains (Fig. 5d), which we believe to represent the amalgamation processes resulting in the aggregation, amalgamation and fusion of small crystals to form lager crystals by the melt flow (e.g., Taylor and Stevens, 2010). The garnet grains commonly show the development of nearly euhedral shapes (Fig. 3), probably as a result of overgrowth of late garnet around the former cores. The rims are characterized by constantly low concentrations of trace elements, which is equilibrated with the melts and depleted by the co-precipitation of beryl, cassiterite, lepidolite and columbite (Fig. 3f-h).

The REE distributions in the core and rim show similar fractionation between LREE and HREE, but the rims are richer in HREE. Both the core and rim have similarly prominently negative Eu anomalies (Fig. 4a). HREE fractionations as monitored by Dy_N/Yb_N and Er_N/Yb_N ratios are discontinuous from cores to rims (Fig. 4b), which is inconsistent with the different partition coefficients $D^{garnet/matrix}$ of $D_{Yb} > D_{Er} > D_{Dy}$, implying that the garnet nucleated in an environment that was depleted in HREE involving the pegmatitic melts. We suspect that the depletion of HREE in the rims may also reflect the dissolution and reprecipitation processes due to the involvement of evolved pegmatitic melts of the same pulse (Fig. 10a-b).

Within individual garnet grains, there are variable patterns of Mn, Mg and Fe zonings, which are typically decoupled from those patterns of most trace elements (Fig. 5d). Calcium is proposed to diffuse slower than

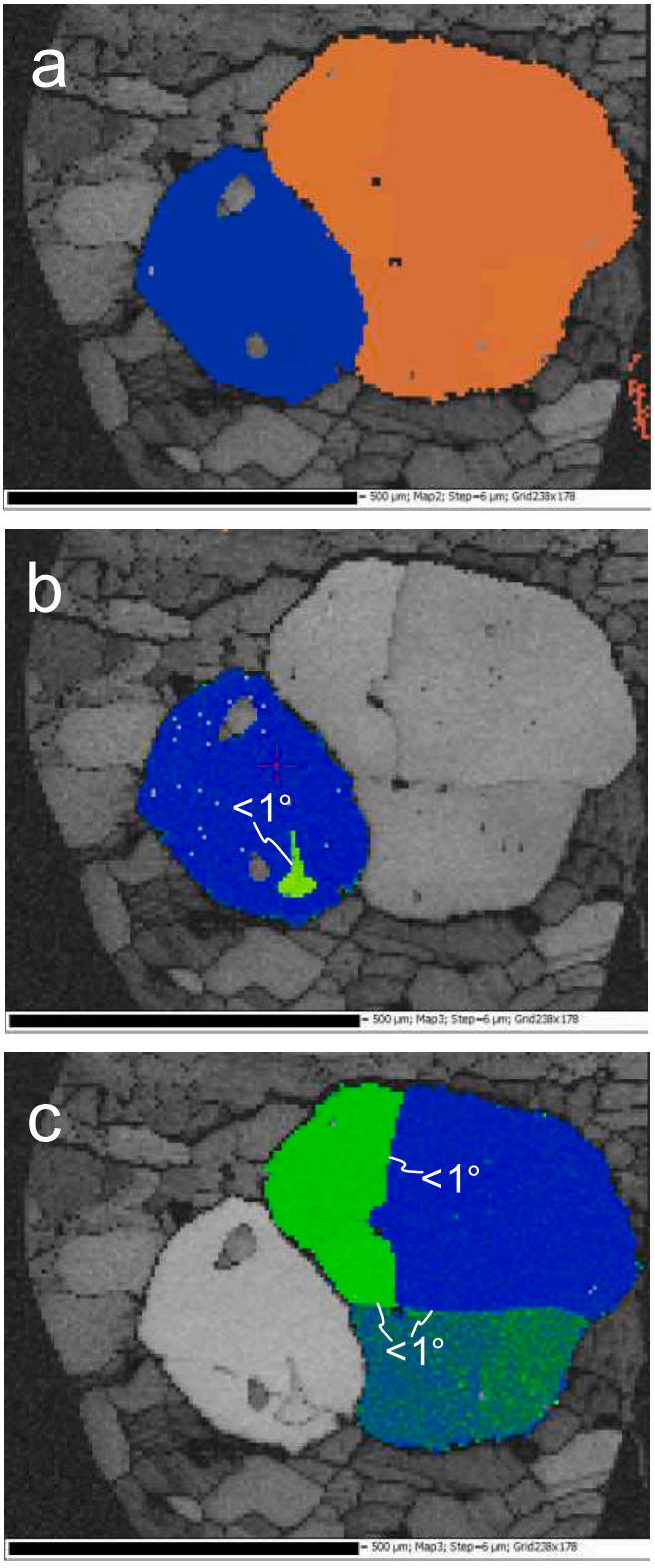

Fig. 7. Orientation contrast images of the garnet grains, which the same grains for mapping as shown in Fig. 5a.

Mn and Fe, but for the garnet grains, Ca is almost homogeneous, indicating that major elements might be homogenized by the intracrystalline diffusion, and the Fe, Mn and Mg zoning patterns could be late-stage features. This assumption is proved by the low-angle crystal boundaries within individual grains revealed by EBSD (Fig. 7), indicating the weak deformation during post- (or possibly syn-) crystallization (Prior et al., 2000). The weak deformation is also reflected by the ductile lineation as shown by the arrangement of albite grains (Fig. 3a,b). During the late-stage deformation, Fe-Mn-Mg were re-organized, but Ca has not been affected due to its lower diffusion rate (Whitney and Seaton, 2010). Previous studies show that higher Fe in garnet may reflect a higher equilibrated temperature (Leake, 1967; Menard and Spear, 1993; Villaros et al., 2009). In Fig. 5d, it shows that the Fe-enriched domains are typically distributed as rims or along those deformed boundaries. It implies that the late-stage deformation, when the fine-grained phases

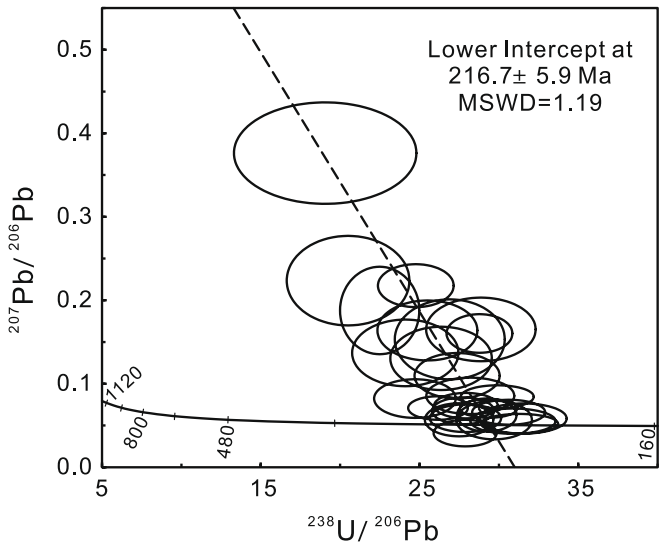

Fig. 8. U–Pb concordia diagrams of garnet from the fine-grained albite phase of the No. 9 dike in the Jiajika deposit.

Table 1
Summery of ages of the Majingzi-Jiajijiami granitic pluton and pegmatite dikes in the Jiajika deposit, eastern Tibet plateau.

		Approaches	Ages	References
Granite	Majingzi	Whole rock-mineral Rb-Sr	214 ± 1.6 Ma	Tang and Wu (1984)
		Zircon U-Pb	223 ± 1 Ma	Hao et al. (2015)
		Zircon U-Pb	212.9 ± 5.9 Ma	Li et al. (2020)
	Jiajijiami	Zircon U-Pb	206.0 ± 3.2 Ma	
Pegmatite	No. 9	Whole rock-mineral Rb-Sr	189.49 ± 3.14 Ma	Tang and Wu (1984)
	No. 134	Muscovite Ar-Ar plateau	195.7 ± 0.1 Ma	Wang et al. (2005)
		Muscovite Ar-Ar isochron	195.4 ± 2.2 Ma	
	No. 104	Muscovite Ar-Ar plateau	198.9 ± 0.4 Ma	
		Muscovite Ar-Ar isochron	199.9 ± 2.3 Ma	
	No. X03	Zircon U-Pb	216 ± 2 Ma	Hao et al. (2015)
		Columbite-tantalite U-Pb	214 ± 2 Ma	
		Zircon U-Pb	186.7 ± 5.3 Ma	Li et al. (2020)
	No.308 fine-grained phase	Zircon U-Pb	217 ± 1.1 Ma	Dai et al. (2019)
	No. 308	Cassiterite U-Pb	211 ± 4.6 Ma	
	No. 133	Cassiterite U-Pb	198.0 ± 4.4 Ma	
	No. 9 fine-grained phase	Garnet U-Pb	217.4 ± 5.7 Ma	This study

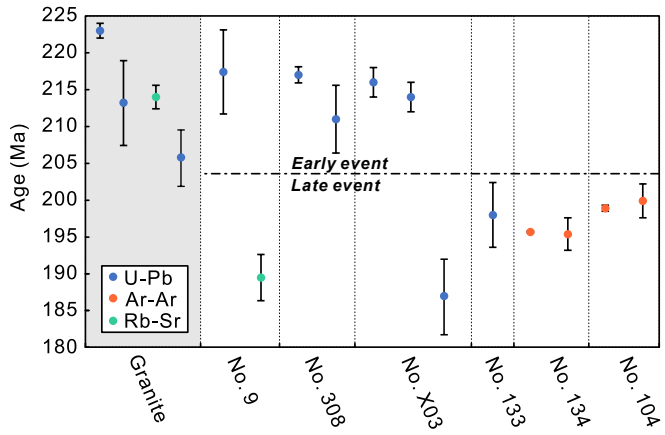

Fig. 9. Plots of published isotopic ages and garnet U-Pb age obtained in this study. Compiled data from Tang and Wu (1984), Wang et al. (2005), Hao et al. (2015), Dai et al. (2019), and Li et al. (2020).

were in solid or semisolid states, could be under a higher temperature condition that that of a simple cooling process. It is suspected to be due to the subsequent emplacement of another pulse of hot melts (Fig. 10c). The different pulses of pegmatitic melts in Jiajika were also initiated by Fu et al. (2019) based on their core loggings and field observations, which is present as precipitation of coarse-grained spodumene assemblage and fine-grained spodumene assemblage. Accordingly, here we, based on compiled dating results, propose that at least two major pulses of pegmatitic were emplaced, which may be correlated to the time spans of ~ 210 Ma to ~ 220 Ma and ~ 190 Ma to ~ 200 Ma (Fig. 9). The second pulse of hot melts would reset the Rb-Sr and Ar-Ar systems resulted from the first pulse, and/or precipitate new muscovite and cassiterite. Although different sizes of spodumene are not significant in the No. 9 dike, two-stage thermal events are recorded by the weak deformation and re-distribution of major elements within garnet grains. However, more work should be carried out in the future to identify and prove the potentially different pulses of pegmatitic melts in Jiajika.

5.3. *Implications for pegmatite formation and Li concentrations in the incipient melts*

Several models have been suggested for the formation of massive and

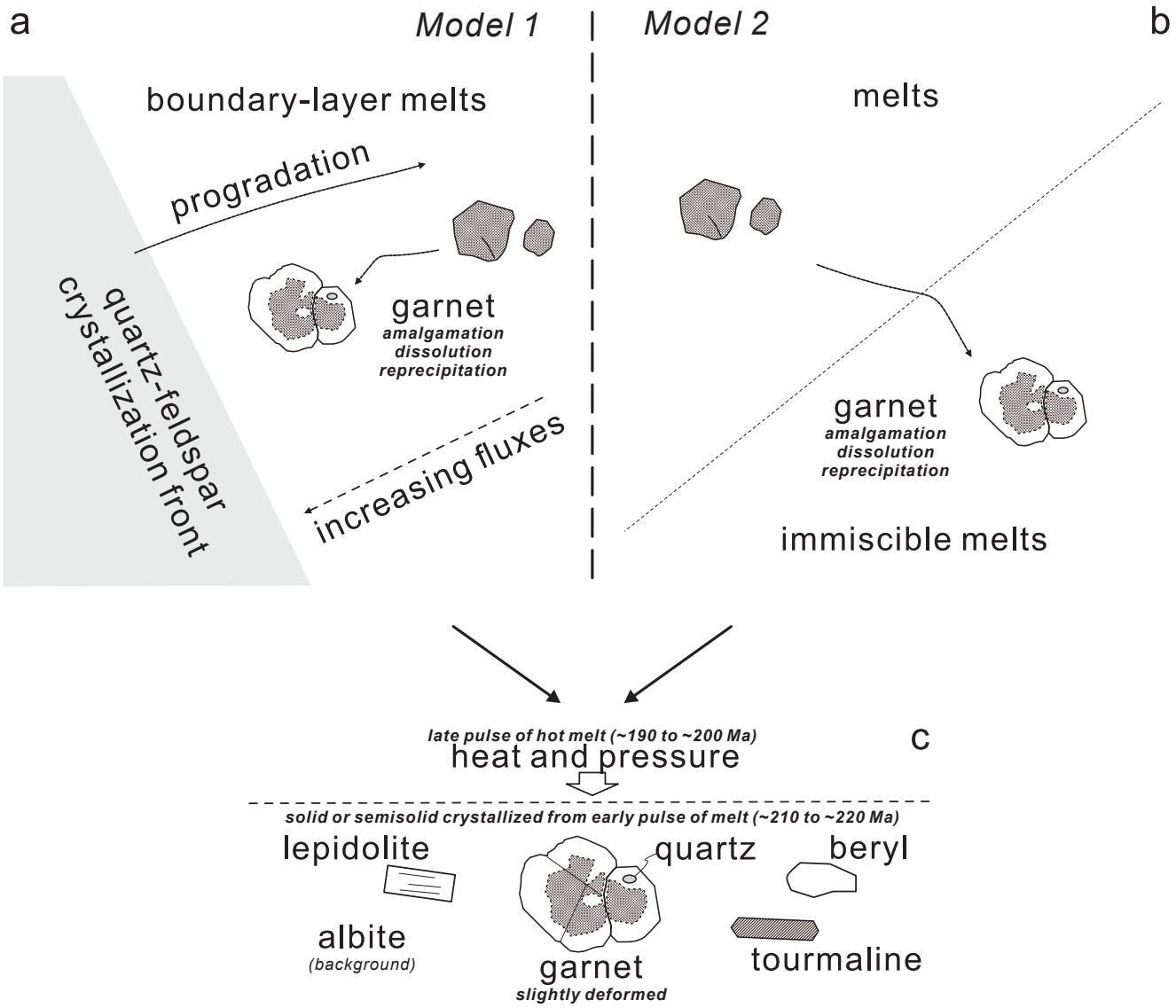

Fig. 10. An illustration of the garnet formation process with the evolution of the incipient pegmatitic melts.

layered fine-grained phases in granitic pegmatites, which may correspond to textural and compositional differences of garnet in pegmatites of the Jiajika deposit. According to Fenn (1986) and London (2005), these fine-grained phases form through kinetic processes (disequilibrium crystallization) at the boundary layer melts adjacent to the rapidly growing quartz-feldspar crystals undercooled by about 100–300 ℃, where increasing concentrations of excluded components can promote the local saturation and precipitation of minerals on adjacent crystal surfaces even if the bulk melts is not saturated in those minerals (Fig. 10a; Model 1). The boundary layer melts are proposed to be flux-rich, including Li, Ta and Nb (Morgan and London, 1999). The solidus of the boundary layer melts is lowered by the fluxes. As crystallization continues, the boundary layer melts become progressively enriched in fluxes, water, and other incompatible elements relative to the bulk melt composition. It is proposed that increased water contents are in favor of the stability of garnet (Harrison, 1988). Therefore, the first-stage garnet (garnet cores) could precipitate in the water-enriched boundary layer melts once the saturation of garnet was reached, and this garnet inherits the flux-rich characteristics of the boundary layer melts. But the subsequent crystallization of ore minerals and other accessory minerals, like tourmaline, might temporally scratch local fluxes, which could reshape the stability of garnet in the evolved boundary layer melts, and cause dissolution and reprecipitation of garnet to form the rim. At this situation, it is reasonable for the local precipitation of quartz (London, 2009), as recorded by the quartz inclusions in garnet rims (Fig. 3e,h and 5b,c). Accordingly, the garnet rims are depleted in trace elements, which might be re-mobilized into the melts and then incorporated in newly-formed minerals.

Alternatively, the fine-grained phases may have formed from different pegmatitic melts, reflecting melt-melt immiscibility. Melt and fluid inclusions of minerals in pegmatites detailed by Thomas et al. (2005) and Webster et al. (1997) suggest that pegmatitic melts may have low viscosity, with high H_2O and diffusivity, and are alkali-rich aluminosilicate in composition (Fig. 10b Model 2). Such melts are able to transport trace and other elements leading to the extreme enrichment of pegmatites in elements such as P, F and B. Based on studies of natural melts and fluid inclusions (Thomas et al., 2012) and experimental work (Thomas and Veksler, 2002), melt-melt immiscibility happened at the early stage of pegmatite formation, which causes the formation of conjugate melt fractions from an exceptionally hydrous and flux-rich primary melt: peraluminous to metaluminous and less water-rich, and alkaline to peralkaline and extremely water-rich. By strong undercooling, the garnet might be precipitated from the extremely hydrous melts, with higher amounts of Li and other rare metals, as the stability of garnet could be more easily reached (Harrison, 1988). Later, the local involvement of the peraluminous to metaluminous immiscible melts might result in the dissolution and precipitation of garnet and co-precipitate quartz, and re-mobilize Li and other trace elements into the melts.

In both models, the garnet cores are interpreted to be out of equilibrium with other phases, while the rims should be re-equilibrated with the subsequent melts and might be progressively equilibrated with other minerals. Accordingly, the Li concentrations in the cores may represent the initial contents in the hydrous melts. The garnet cores in this study generally have ~ 350 ppm Li (Fig. 4c and 6). Although Li partition coefficients are unavailable for garnet/granitic melts, Li is generally an incompatible element for garnet (Bennett et al., 2004; Elkins et al., 2008; Klemme et al., 2006; van Westrenen et al., 2000; Yurimoto and Ohtani, 1992), and thus it is reasonable that the incipient pegmatitic melts for precipitation of garnet cores had thousands of ppm Li, which could be distinctively higher than the average content (~335 ppm Li) of other Li-rich pegmatites (Stewart, 1978). In the $NaAlSi_3O_8$-$LiAlSiO_4$-SiO_2-H_2O system, Stewart (1978) illustrated that hydrous silicate liquids should contain ~ 1.8 wt% Li_2O on the liquidus surface at 200 MPa that could be saturated in Li ore minerals. Accordingly, our results show that, although different models could be involved, Li and other incompatible element contents of the incipient pegmatitic melts in Jiajiaka could be enriched in a significant amount at the early stage, which may, to some extent, explain why major Li resources are hosted in very-fine to fine-grained phases in Jiajika.

6. Conclusions

The in-situ U-Pb age of 216.7 ± 5.9 Ma for pegmatite garnet from the fine-grained phase of the No. 9 dike in the Jiajika deposit is similar to the age of the Majingzi-Jiajijiami granitic pluton. The textural features, and major and trace elemental patterns of garnet show that the garnet cores might be precipitated from hydrous melts by strong undercooling and out of equilibrium with other phases. Then the grains experienced amalgamation, dissolution and reprecipitation with the evolution of the pegmatitic melts. The late-stage deformation by the emplacement of second pulse of hot melts reset the major element patterns. Overall, our findings imply that the incipient pegmatitic melts contained significant amounts of Li, which was potentially responsible for the accumulation of major Li in fine-grained phases to form the Jiajika deposit.

Declaration of Competing Interest

The authors declare that they have no known competing financial interests or personal relationships that could have appeared to influence the work reported in this paper.

Data availability

Data will be made available on request.

Acknowledgments

The study is supported by the National Science Foundation of China (42102090) and Fundamental Research Funds for the Central Universities, China University of Geosciences (Wuhan) (CUG2106104) to WWZ, and Geological Survey Project of China Geological Survey (No. DD20221684) to ZZ. We are grateful to Shanbao Liu, Hui Zhang, Pingping Liu, Wei Terry Chen, Fangyue Wang, Junpeng Wang, Chang Xu, Yanwen Tang, Junjie Han and Tao Luo for their initial discussions, and field and technical supports. This manuscript was significantly improved with constructive reviews by Editors Huayong Chen and Hongrui Fan, and two anonymous referees.

Appendix A. Supplementary data

Supplementary data to this article can be found online at https://doi.org/10.1016/j.oregeorev.2023.105484.

References

Arredondo, E.H., Rossman, G.R., Lumpkin, G.R., 2001. Hydrogen in spessartine-almandine garnets as a tracer of granitic pegmatite evolution. American Mineralogist 86 (4), 485–490.

Baldwin, J.R., von Knorring, O., 1983. Compositional range of Mn-garnet in zoned granitic pegmatites. Canadian Mineralogist 21, 683–688.

Bennett, S.L., Blundy, J., Elliott, T., 2004. The effect of sodium and titanium on crystal-melt partitioning of trace elements. Geochimica et Cosmochimica Acta 68 (10), 2335–2347.

Bonzi, W.-M.-E., Van Lichtervelde, M., Vanderhaeghe, O., André-Mayer, A.-S., Salvi, S., Wenmenga, U., 2023. Insights from mineral trace chemistry on the origin of NYF and mixed LCT + NYF pegmatites and their mineralization at Mangodara. SW Burkina Faso. Mineralium Deposita 58 (1), 75–104.

Černý, P., Blevin, P., Cuney, M., London, D., 2005. Granite-related ore deposits. Society of Economic Geologists 100, 337–370.

Chakraborty, S., Ganguly, J., 1992. Cation diffusion in aluminosilicate garnets: experimental determination in spessartine-almandine diffusion couples, evaluation of effective binary diffusion coefficients, and applications. Contributions to Mineralogy and Petrology 111 (1), 74–86.

Chiaradia, M., Schaltegger, U., Spikings, R., Wotzlaw, J.F., Ovtcharova, M., 2013. How accurately can we date the duration of magmatic-hydrothermal events in porphyry systems?-An invited paper. Economic Geology 108 (4), 565–584.

Dai, H.Z., Wang, D.H., Liu, L.J., Yu, Y., Dai, J.J., 2019. Geochronology and Geochemistry of Li(Be)-Bearing Granitic Pegmatites from the Jiajika Superlarge Li-Polymetallic Deposit in Western Sichuan. China. Journal of Earth Science 30 (4), 707–727.
Deng, J., Li, J., Zhang, D., Chou, I.-M., Yan, Q., Xiong, X., 2022. Origin of pegmatitic melts from granitic magmas in the formation of the Jiajika lithium deposit in the eastern Tibetan Plateau. Journal of Asian Earth Sciences 229, 105147.
Elkins, L.J., Gaetani, G.A., Sims, K.W.W., 2008. Partitioning of U and Th during garnet pyroxenite partial melting: Constraints on the source of alkaline ocean island basalts. Earth and Planetary Science Letters 265 (1), 270–286.
Fenn, P.M., 1986. On the origin of graphic granite. American Mineralogist 71 (3–4), 325–330.
Fu, X.F., Hou, L.W., Ruan, L.S., Liang, B., Hao, X.F., Yuan, L.P., Wang, D.H., Zhao, C., Zou, F.G., Pan, M., Tang, Y., Huang, T., Xiao, R.Q., Yang, R., Feng, Y.D., Zhang, C., 2019. Emerging critical mineral resources: Introduction to the development and utilization of rare and rare earth scattered resources in Sichuan Province. Science Press, Beijing.
George, F.R., Gaidies, F., Boucher, B., 2018. Population-wide garnet growth zoning revealed by LA-ICP-MS mapping: implications for trace element equilibration and syn-kinematic deformation during crystallisation. Contribution to Mineralogy and Petrology 173, pp. 1–22.
Hao, X.F., Fu, X.F., Liang, B., Yuan, L.P., Pan, M., Tang, Y., 2015. Formation Ages of Granite and X03 Pegmatite Vein in Jiajika, Western Sichuan, and Their Geological Significance. Mineral Deposits 34 (6), 1199–1208.
Harrison, T.N., 1988. Magmatic Garnets in the Cairngorm Granite. Scotland. Mineralogical Magazine 52 (368), 659–667.
Klemme, S., Günther, D., Hametner, K., Prowatke, S., Zack, T., 2006. The partitioning of trace elements between ilmenite, ulvospinel, armalcolite and silicate melts with implications for the early differentiation of the moon. Chemical Geology 234 (3), 251–263.
Leake, B.E., 1967. Zoned garnets from the Galway granite and its aplites. Earth and Planetary Science Letters 3, 311–316.
Li, J., Chou, I.M., 2015. Hydrogen in silicate melt inclusions in quartz from granite detected with Raman spectroscopy. Journal of Raman Spectroscopy 46 (10), 983–986.
Li, J.K., Chou, I.M., 2016. An occurrence of metastable cristobalite in spodumene-hosted crystal-rich inclusions from Jiajika pegmatite deposit, China. Journal of Geochemical Exploration 171, 29–36.
Li, J., Chou, I.-M., 2017. Homogenization Experiments of Crystal-Rich Inclusions in Spodumene from Jiajika Lithium Deposit, China, under Elevated External Pressures in a Hydrothermal Diamond-Anvil Cell. Geofluids 2017, 1–12.
Li, J., Li, S., 2014. Application of Hydrothermal Diamond Anvil Cell to Homogenization Experiments of Silicate Melt Inclusions. Acta Geologica Sinica - English Edition 88 (3), 854–864.
Li, X.F., Tian, S.H., Wang, D.H., Zhang, H.J., Zhang, Y.J., Fu, X.F., Hao, X.F., Hou, K.J., Zhao, Y., Qin, Y., Yu, Y., Wang, H., 2020. Genetic relationship between pegmatite and granite in Jiajika lithium deposit in western Sichuan: Evidence from zircon U-Pb dating. Hf-O isotope and geochemistry. Mineral Deposits 39 (2), 273–304.
Liang, B., Fu, X., Tang, Y., Pan, M., Yuan, L., Hao, X., 2016. Granite geochemical characteristics in Jiajika rare metal deposit, western Sichuan. Journal of Guilin University of Technology 36 (1), 42–49.
Linnen, R.L., Van Lichtervelde, M., Černý, P., 2012. Granitic pegmatites as sources of strategic metals. Elements 8 (4), 275–280.
Liu, Y., Hu, Z., Zong, K., Gao, C., Gao, S., Xu, J., Chen, H., 2010. Reappraisement and refinement of zircon U-Pb isotope and trace element analyses by LA-ICP-MS. Chinese Science Bulletin 55 (15), 1535–1546.
London, D., 2005. Granitic pegmatites: an assessment of current concepts and directions for the future. Lithos 80 (1–4), 281–303.
London, D., 2009. THE ORIGIN OF PRIMARY TEXTURES IN GRANITIC PEGMATITES. The Canadian Mineralogist 47 (4), 697–724.
London, D., 2014. A petrologic assessment of internal zonation in granitic pegmatites. Lithos 184, 74–104.
London, D., 2016. Rare Earth and Critical Elements in Ore Deposits. Society of Economic Geologists.
Ludwig, R.K., 2001. User Manual for Isoplot/ Ex rev. 2.49. Berkeley Geochronology Center Special Publication, 1a. Berkeley Geochronology Center, Berkeley, CA.
Maneta, V., Baker, D.R., Minarik, W., 2015. Evidence for lithium-aluminosilicate supersaturation of pegmatite-forming melts. Contributions to Mineralogy and Petrology 170 (1), 4.
Manning, D.A.C., 1983. Chemical variation in garnets from aplites and pegmatites, peninsular Thailand. Mineralogical Magazine 47 (344), 353–358.
Menard, T., Spear, F.S., 1993. Metamorphism of calcic pelitic schists, Strafford Dome, Vermont: compositional zoning and reaction history. Journal of Petrology 34 (5), 977–1005.
Morgan, G.B., London, D., 1999. Crystallization of the Little Three layered pegmatite-aplite dike, Ramona District. California. Contributions to Mineralogy and Petrology 136 (4), 310–330.
Ning, S., Wang, F., Xue, W., Zhou, T., 2017. Geochemistry of the Baoshan pluton in the Tongling region of the Lower Yangtze River Belt. Geochimica 46 (5), 397–412.
Ning, W.B., Wang, J.P., Xiao, D., Li, F.F., Huang, B., Fu, D., 2019. Electron Probe Microanalysis of Monazite and Its Applications to U-Th-Pb Dating of Geological Samples. Journal of Earth Science 30 (5), 952–963.
Prior, D.J., 1999. Problems in determining the orientations of crystal misorientation axes, for small angular misorientations, using electron backscatter diffraction in the SEM. Journal of Microscopy 195, 217–225.
Prior, D.J., Wheeler, J., Brenker, F.E., Harte, B., Matthews, M., 2000. Crystal plasticity of natural garnet: New microstructural evidence. Geology 28 (11), 1003–1006.
Putnis, A., 2009. Mineral replacement reactions. Reviews in mineralogy and geochemistry 70 (1), 87–124.
Pyle, J.M., Spear, F.S., 2003. Yttrium zoning in garnet: Coupling of major and accessory phases during metamorphic reactions. American Mineralogist, 88(4): 708-708.
Roger, F., Calassou, S., Lancelot, J., Malavieille, J., Mattauer, M., Zhiqin, X., Ziwen, H., Liwei, H., 1995. Miocene emplacement and deformation of the Konga Shan granite (Xianshui He fault zone, west Sichuan, China): Geodynamic implications. Earth and Planetary Science Letters 130 (1), 201–216.
Roger, F., Jolivet, M., Malavieille, J., 2010. The tectonic evolution of the Songpan-Garzê (North Tibet) and adjacent areas from Proterozoic to Present: A synthesis. Journal of Asian Earth Sciences 39 (4), 254–269.
Samadi, R., Miller, N.R., Mirnejad, H., Harris, C., Kawabata, H., Shirdashtzadeh, N., 2014. Origin of garnet in aplite and pegmatite from Khajeh Morad in northeastern Iran: A major, trace element, and oxygen isotope approach. Lithos 208–209, 378–392.
Seman, S., Stockli, D.F., McLean, N., 2017. U-Pb geochronology of grossular-andradite garnet. Chemical Geology 460, 106–116.
Simmons, W.B.S., Webber, K.L., 2008. Pegmatite genesis: state of the art. European Journal of Mineralogy 20 (4), 421–438.
Stevens, G., Villaros, A., Moyen, J.-F.o., 2007. Selective peritectic garnet entrainment as the origin of geochemical diversity in S-type granites. Geology, 35(1): 9-12.
Spandler, C., Pettke, T., Rubatto, D., 2011. Internal and external fuid sources for eclogite-facies veins in the Monviso meta-ophiolite, Western Alps: implications for fuid fow in subduction zones. Journal of Petrology 52, 1207–1236.
Stewart, D.B., 1978. Petrogenesis of lithium-rich pegmatites. American Mineralogist 63 (9–10), 970–980.
Sun, S.-S., McDonough, W.-S., 1989. Chemical and isotopic systematics of oceanic basalts: implications for mantle composition and processes. Geological Society, London, Special Publications 42 (1), 313–345.
Tang, Y., Gao, J., Lan, T., Cui, K., Han, J., Zhang, X., Chen, Y., Chen, Y., 2021. In situ low-U garnet U-Pb dating by LA-SF-ICP-MS and its application in constraining the origin of Anji skarn system combined with Ar-Ar dating and Pb isotopes. Ore Geology Reviews 130, 103970.
Tang, G.F., Wu, S.X., 1984. Geological reports on the Jiajika pegmatite Li deposit in Kangding. Sichuan Province, Sichuan Bureau of Geology and Resources, Chengdu, p. 104.
Taylor, J., Stevens, G., 2010. Selective entrainment of peritectic garnet into S-type granitic magmas: Evidence from Archaean mid-crustal anatectites. Lithos 120 (3), 277–292.
Thomas, R., Förster, H.-J., Rickers, K., Webster, J.D., 2005. Formation of extremely F-rich hydrous melt fractions and hydrothermal fluids during differentiation of highly evolved tin-granite magmas: a melt/fluid-inclusion study. Contributions to Mineralogy and Petrology 148 (5), 582–601.
Thomas, R., Davidson, P., Beurlen, H., 2012. The competing models for the origin and internal evolution of granitic pegmatites in the light of melt and fluid inclusion research. Mineralogy and Petrology 106 (1), 55–73.
Thomas, R., Veksler, I., 2002. Formation of granite pegmatites in the light of melt and fluid inclusion studies and new and old experimental work. Mineralogical Society of Poland Special Papers 20, 44–49.
van Westrenen, W., Blundy, J.D., Wood, B.J., 2000. Effect of Fe 2+ on garnet–melt trace element partitioning: experiments in FCMAS and quantification of crystal-chemical controls in natural systems. Lithos 53 (3), 189–201.
Villaros, A., Stevens, G., Buick, I.S., 2009. Tracking S-type granite from source to emplacement: Clues from garnet in the Cape Granite Suite. Lithos 112 (3), 217–235.
Wang, R.C., Fontan, F., Chen, X.M., Hu, H., Liu, C.S., Xu, S.J., de Parseval, P., 2003b. Accessory minerals in the Xihuashan Y-enriched granitic complex, southern China: a record of magmatic and hydrothermal stages of evolution. The Canadian Mineralogist 41 (3), 727–748.
Wang, F., Ge, G., Ning, S., Nie, L., Zhong, G., White, N.C., 2017. A new approach to LA-ICP-MS mapping and application in geology. Acta Petrologica Sinica 33 (11), 3422–3436.
Wang, R., Hu, H., Zhang, A., Xu, S., Wang, D., 2003a. Yttrium zoning in garnet from the Xihuashan granitic complex and its petrological implications. Chinese Science Bulletin 48 (15), 1611–1615.
Wang, D.H., Li, J.K., Fu, X.F., 2005. 40Ar/39Ar dating for the Jiajika pegmatite-type rare metal deposit in western Sichuan and its significance. Geochimica(6), 541–547.
Wang, J.P., Li, X.W., Ning, W.B., Kusky, T.M., Wang, L., Polat, A., Deng, H., 2019. Geology of a Neoarchean suture: Evidence from the Zunhua ophiolitic melange of the Eastern Hebei Province, North China Craton. Geological Society of America Bulletin 131 (11–12), 1943–1964.
Webster, J.D., Thomas, R., Rhede, D., Förster, H.-J., Seltmann, R., 1997. Melt inclusions in quartz from an evolved peraluminous pegmatite: Geochemical evidence for strong tin enrichment in fluorine-rich and phosphorus-rich residual liquids. Geochimica et Cosmochimica Acta 61 (13), 2589–2604.
Whitney, D.L., Seaton, N.C.A., 2010. Garnet polycrystals and the significance of clustered crystallization. Contributions to Mineralogy and Petrology 160 (4), 591–607.
Whitworth, M.P., 1992. Petrogenetic implications of Garnets Associated with lithium pegmatites from SE Ireland. Mineralogical Magazine 56 (382), 75–83.
Xiao, X., Zhou, T.-F., White, N.C., Zhang, L.-J., Fan, Y., Wang, F.-Y., Chen, X.-F., 2018. The formation and trace elements of garnet in the skarn zone from the Xinqiao Cu-S-Fe-Au deposit, Tongling ore district, Anhui Province, Eastern China. Lithos 302, 467–479.
Xu, Z., Fu, X., Wang, R., Li, G., Zheng, Y., Zhao, Z., Lian, D., 2020. Generation of lithium-bearing pegmatite deposits within the Songpan-Ganze orogenic belt. Lithos 354-355, 105281.

Xu, Z.Q., Hou, L.W., Wang, Z.X., Fu, X.F., Huang, M.H., 1992. Orogenic processes of the Songpan-Garze orogenic belt of China. Geology Publishing House, Beijing, p. 235.
Yin, A., Harrison, T.M., 2000. Geologic Evolution of the Himalayan-Tibetan Orogen. Annual Review of Earth and Planetary Sciences 28 (1), 211–280.
Yu, M., Xia, Q.X., Zheng, Y.F., Zhao, Z.F., Chen, Y.X., Chen, R.X., Luo, X., Li, W.C., Xu, H. J., 2021. The composition of garnet in granite and pegmatite from the Gangdese orogen in southeastern Tibet: Constraints on pegmatite petrogenesis. American Mineralogist 106 (2), 265–281.
Yuan, C., Zhou, M.-F., Sun, M., Zhao, Y., Wilde, S., Long, X., Yan, D., 2010. Triassic granitoids in the eastern Songpan Ganzi Fold Belt, SW China: Magmatic response to geodynamics of the deep lithosphere. Earth and Planetary Science Letters 290 (3), 481–492.
Yurimoto, H., Ohtani, E., 1992. Element partitioning between majorite and liquid: A secondary ion mass spectrometric study. Geophysical Research Letters 19 (1), 17–20.
Zhang, H., Tian, S., Wang, D., Li, X., Liu, T., Zhang, Y., Fu, X., Hao, X., Hou, K., Zhao, Y., Qin, Y., 2021. Lithium isotope behavior during magmatic differentiation and fluid exsolution in the Jiajika granite-pegmatite deposit. Ore Geology Reviews 134, 104139.
Zhao, H., Chen, B., Huang, C., Bao, C., Yang, Q., Cao, R., 2022. Geochemical and Sr-Nd-Li isotopic constraints on the genesis of the Jiajika Li-rich pegmatites, eastern Tibetan Plateau: implications for Li mineralization. Contributions to Mineralogy and Petrology 177 (1).